Inversion of high frequency surface waves with fundamental and higher modes

Article *in* Journal of Applied Geophysics · January 2003

DOI: 10.1016/S0926-9851(02)00239-2

Available online at www.sciencedirect.com
SCIENCE DIRECT®
Journal of Applied Geophysics 52 (2003) 45–57
JOURNAL OF APPLIED GEOPHYSICS
www.elsevier.com/locate/jappgeo

Inversion of high frequency surface waves with fundamental and higher modes

Jianghai Xia[a,*], Richard D. Miller[a], Choon B. Park[a], Gang Tian[b]

[a] *Kansas Geological Survey, The University of Kansas, 1930 Constant Avenue, Campus West, Lawrence, KS 66047-3726, USA*
[b] *Department of Geophysics, Jinlin University, People's Republic of China*

Received 17 October 2001; accepted 24 October 2002

Abstract

The phase velocity of Rayleigh-waves of a layered earth model is a function of frequency and four groups of earth parameters: compressional (P)-wave velocity, shear (S)-wave velocity, density, and thickness of layers. For the fundamental mode of Rayleigh waves, analysis of the Jacobian matrix for high frequencies (2–40 Hz) provides a measure of dispersion curve sensitivity to earth model parameters. S-wave velocities are the dominant influence of the four earth model parameters. This thesis is true for higher modes of high frequency Rayleigh waves as well. Our numerical modeling by analysis of the Jacobian matrix supports at least two quite exciting higher mode properties. First, for fundamental and higher mode Rayleigh wave data with the same wavelength, higher modes can "see" deeper than the fundamental mode. Second, higher mode data can increase the resolution of the inverted S-wave velocities. Real world examples show that the inversion process can be stabilized and resolution of the S-wave velocity model can be improved when simultaneously inverting the fundamental and higher mode data.

Keywords: Surface waves; Higher modes; Shear wave velocity; Resolution; Inversion

1. Introduction

Elastic properties of near-surface materials (such as soil, rocks, and pavement) and their effects on seismic wave propagation are of fundamental interest in groundwater, engineering, and environmental studies. For example, Imai and Tonouchi (1982) studied compressional (P)- and shear (S)-wave velocities in an embankment, and also in alluvial, diluvial, and Tertiary layers, showing that S-wave velocities in such deposits possess a direct relationship to the N-value (Craig, 1992), an index value of formation hardness used in soil mechanics and foundation engineering. S-wave velocity is used to determine "stiffness", one of the key earth properties in construction engineering. S-wave velocity as a function of depth can be derived from inverting the phase velocity of the surface (Rayleigh and/or Love) wave (Dorman and Ewing, 1962).

Surface waves are guided and dispersive. Rayleigh waves (1885) are surface waves that travel along a "free" surface, such as the earth–air interface, and are the result of interfering P and S_v waves. Particle

* Corresponding author. Tel.: +86-785-864-2057; fax: +86-785-864-5317.
E-mail address: jxia@kgs.ku.edu (J. Xia).

0926-9851/02/$ - see front matter © 2002 Elsevier Science B.V. All rights reserved.
PII: S0926-9851(02)00239-2

motion of Rayleigh waves moving from left to right is elliptical in a counterclockwise (retrograde) direction in a homogeneous medium. This motion is constrained to a vertical plane in the direction of wave propagation (p. 30, Babuska and Cara, 1991). Theoretically, Rayleigh waves only propagate along a free boundary plane in a semi-infinite and homogeneous medium. In the case of surface layers of variable thickness overlying a substratum, as discussed in this paper, waves propagating along the surface are pseudo-Rayleigh waves. However, we will still use the term Rayleigh waves throughout this paper to simplify our terminology. Longer wavelengths (lower frequency components) penetrate deeper than shorter wavelengths (higher frequency components) for a given mode, in general exhibit greater phase velocities, and are more sensitive to the elastic properties of deeper layers (p. 30, Babuska and Cara, 1991). Shorter wavelengths are sensitive to the physical properties of surficial layers. For this reason, surface waves possess a variation of velocity with frequency, which results in dispersion characteristics.

Ground roll is a particular type of Rayleigh wave that travels along or near the ground surface and is usually characterized by a relatively low velocity, low frequency, and high amplitude (p. 143, Sheriff, 1991). Stokoe and Nazarian (1983) have presented a surface-wave method, Spectral Analysis of Surface Waves (SASW), that utilized a two-channel recording system and analyzes the fundamental mode dispersion curve of ground roll to produce near-surface S-wave velocity profiles. There are several other groups of researchers also working on estimating S-wave velocity from Rayleigh waves. Malagnini et al. (1995) derived S-wave velocity and Q structure of Quaternary alluvium from Rayleigh waves. In a similar work, Mattews et al. (1996) find that an S-wave velocity-depth profile can be determined from dispersion curves. Glangeaud et al. (1999) analyzed Love, Rayleigh, and Stoneley waves in different civil engineering studies.

A research group at the Kansas Geological Survey (KGS) investigated how to estimate the S-wave velocity of near-surface materials from ground roll with a multi-channel recording system, focusing mainly on the fundamental mode of Rayleigh waves. The resulting technique consists of: (1) acquisition of wide band, high frequency ground roll using a multi-channel recording system; (2) creation of efficient and accurate algorithms designed to extract multi-modal Rayleigh-wave dispersion curves from ground roll using a basic, robust, and pseudoautomated processing sequence (Park et al., 1999a); (3) development of stable and efficient inversion algorithms to obtain S-wave velocity profiles (Xia et al., 1999), and (4) applications of characterization of near-surface materials by S-wave velocity field. The main products of this research, called Multi-channel Analysis of Surface Waves (MASW), have been published by Park et al. (1996, 1998, 1999a), Xia et al. (1997, 1998, 1999, 2000), and Miller et al. (1999).

In this paper, we focus our attention on higher modes of high frequency Rayleigh waves. A series of Rayleigh waves of different frequencies can have the same wave velocity. These different frequency Rayleigh waves for a given phase velocity are known as modes and are characterized by their different number of horizontal nodal planes (planes of no particle displacement within the layer) (p. 60, Garland, 1979). In other words, more than one phase velocity can be associated with a given frequency of Rayleigh wave simply because these waves can travel at different velocities for a given frequency. The lowest velocity for any given frequency is called the fundamental mode velocity (or the first mode). The next velocity higher than the fundamental mode phase velocity is called the second mode velocity, and so on. All phase velocities that are higher than the fundamental mode velocities are called higher modes.

Based on our experience, when calculated with high accuracy, the fundamental mode phase velocities can generally provide reliable S-wave velocities with relative error less than $\pm$ 15% (Xia et al., 1999, 2000, 2002a, 2002b). However, in cases where estimations of the fundamental mode phase velocities are associated with high degree of error (e.g., if the fundamental mode of Rayleigh waves is contaminated by body waves and/or higher modes of Rayleigh waves), the inversion process will become unstable. It is well known that instability in the inversion of geophysical data generally results in situations where small changes in data result in large fluctuations in a model. This instability could be reduced either by imposing constraints or by including an extra independent data set in the inversion procedure.

Higher modes are independent from the fundament-mode phase velocities. They exist under a spe-

cific frequency condition (Aki and Richards, 1980). It has been reported that the generation of higher modes has been associated with presence of a velocity reversal (a lower S-wave velocity layer between higher S-wave velocity layers) (Stokoe et al., 1994) and that higher mode surface waves, when trapped in a layer, are much more sensitive to the fine structure of the S-wave velocity field (Kovach, 1965). Reliable observation of higher modes is possible with multichannel recording. A new technique (Park et al., 1999b) allows direct construction of a high-resolution image of multimodal dispersion curves from multichannel records with a relatively small number of traces (e.g., 30 traces) covering only a small lateral distance (20 m). Observations of higher modes of Rayleigh waves using the MASW method have been reported (Park et al., 1999b,c).

The other reason that we must utilize higher modes is that in some situations higher modes take more energy than the fundamental mode does in a higher frequency range, which means the fundamental mode data may not be available in the higher frequency range and higher modes are the only choice. We can demonstrate this property as shown in Fig. 1. Energy of the fundamental mode is much less than higher modes when frequencies are higher than 17 Hz. Higher modes are necessity in this case to obtain an accurate S-wave velocity profile.

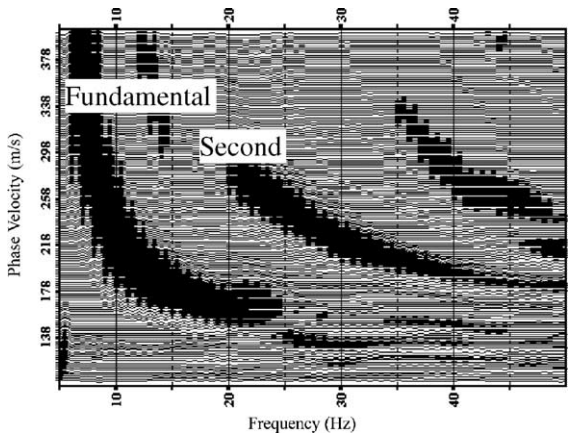

Fig. 1. An example of higher modes. The fundamental and the second mode dispersive curves are clearly shown. The image was generated from the raw field data shown in Fig. 7a. Energy of the second mode is much higher than energy of the fundamental mode when frequencies are higher than 17 Hz.

Xia et al. (1999) discussed properties of the fundamental mode surface wave data and presented efficient inversion algorithms to obtain S-wave velocity profiles from the fundamental mode surface wave data. Inversion of the fundamental and higher mode data simultaneously has nothing special in terms of inversion algorithms except for including higher mode data in the inversion process as an extra set of data with equal weighting or different weighting dependent on data accuracy. The algorithms presented in Xia et al. (1999) were employed to invert the surface wave data shown in this paper. In the following sections, we first analyze the Jacobian matrix to show advantages of utilizing higher modes in inversion of surface wave data. Then, we use two real-world examples to demonstrate the advantages. One real-world example also demonstrates that if no constraints or extra data are available, the inversion can be stabilized by reducing the resolution of the inverted S-wave velocity model.

2. Modeling results

The Rayleigh-wave phase velocity of a layered earth model is a function of frequency and four groups of earth parameters: P-wave velocity, S-wave velocity, density, and thickness of layers. Rayleigh wave dispersion curves can be calculated by Knopoff's method (Schwab and Knopoff, 1972). Rayleigh wave phase velocity, c_{Rj}, is determined by a characteristic equation F, in its nonlinear, implicit form:

$$F(f_j, c_{Rj}, \mathbf{v}_s, \mathbf{v}_p, \rho, \boldsymbol{h}) = 0 \, (j = 1, 2, \ldots, m), \qquad (1)$$

where f_j is the frequency in Hz, c_{Rj} is the Rayleigh wave phase velocity at frequency of f_j, $\mathbf{v}_s=(v_{s1}, v_{s2}, \ldots, v_{sn})^T$ is the S-wave velocity vector with v_{si} the shear wave velocity of the ith layer, n is the number of layers, $\mathbf{v}_p=(v_{p1}, v_{p2}, \ldots, v_{pn})^T$ is the P-wave velocity vector with v_{pi} the P-wave velocity of the ith layer, $\rho=(\rho_1, \rho_2, \ldots,\rho_n)^T$ is the density vector with ρ_i the density of the ith layer, and $\boldsymbol{h}=(h_1, h_2, \ldots, h_{n-1})^T$ is the thickness vector with h_i the thickness of the ith layer. Given a set of model parameters ($\mathbf{v}_s$, $\mathbf{v}_p$, ρ, and $\boldsymbol{h}$) and a specific frequency (f_j), the roots of Eq. (1) are the phase velocities. If the dispersion curve consists of m data points, a set of m equations in the form

of Eq. (1) can be used to find phase velocities at frequencies f_j ($j=1, 2, \ldots, m$) using the bisection method (p. 350, Press et al., 1992).

Xia et al. (1999) analyzed the Jacobian matrix of Rayleigh-wave phase velocity function (1) and found that the ratio of changes in phase velocity to changes in S-wave velocity is around 1.5 and the ratio of changes in phase velocity to other properties are much less than one. Xia et al. (1999) numerically confirmed that S-wave velocity is the dominant property for the fundamental mode of high-frequency Rayleigh wave dispersion data (Aki and Richards, 1980). The influence of earth parameters on the dispersion curves is treated in detail by Aki and Richards (1980, p. 291). We will incorporate the model (Xia et al., 1999, Fig. 2) to numerically analyze: (1) sensitivity of higher modes of high frequency surface waves, (2) the relationship between investigation depth and wavelength of higher mode surface waves, and (3) stability during inversion with higher modes.

Contributions to the higher mode Rayleigh-wave phase velocity from each parameter were calculated as a 25% change in a particular parameter. Table 1 summarizes sensitivity of dispersion curve to model parameters. First, second, and third in Table 1 refer to the fundamental, the second, and the third mode Raleigh wave data, respectively. A 25% change in S-wave velocity causes a 40% and 36% changes in the second and the third modes, respectively (Fig. 3 and Table 1). Furthermore, a 25% change in P-wave velocity and/or, density causes only an 8% change in the second mode and virtually no change in the third mode Rayleigh wave data. The effect of layer thickness on Rayleigh-wave data can be minimized by subdividing certain thinner layers within each constant S-wave velocity slice. Based on this analysis and results reported by Xia et al. (1999), only S-wave velocities are left as unknowns in our inverse procedure. With the lack of sensitivity of the Rayleigh wave to P-wave velocities and densities, estimations of S-wave velocities can be made for a layered earth model.

Table 1
Change of phase velocities in percentage due to a 25% change in model parameters

Parameters	Model (%)	First (%)	Second (%)	Third (%)
P-wave velocity	25	3	1	1
Density	25	10	8	1
S-wave velocity	25	39	40	36
Thickness	25	16	11	14

First, second, and third (%) represent percentage changes in the fundamental, the second mode, and the third mode phase velocities, respectively.
Results in the column "first (%)" are from Xia et al., 1999.

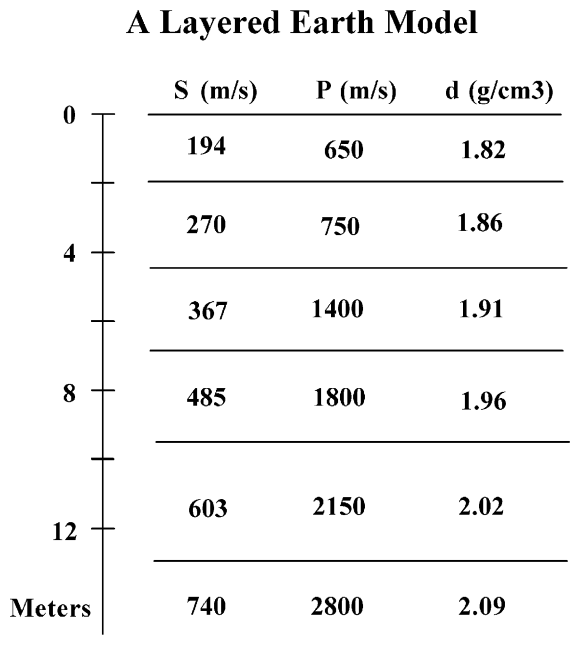

Fig. 2. This 6-layer model (Xia et al., 1999) is used to analyze properties of higher modes of high frequency Rayleigh waves. S, P, and d represent S-wave velocity, P-wave velocity, and density, respectively.

The penetrating depth of surface waves is limited by a wavelength of a surface-wave component. Grant and West (1962 p. 79) pointed out that as modes increase, the penetration of energy into deeper layer becomes progressively easier, with the result that the interface appears to become decreasingly "rigid" to the higher modes. We used the Jacobian matrix of Eq. (1) to analyze the penetrating depth. One element of the Jacobian matrix is the rate of change in a phase velocity at certain frequency in response to changes in an S-wave velocity of a particular layer. That the element of the Jacobian matrix is close to zero indicates that changes in a phase velocity of the corresponding frequency due to changes in a related S-wave velocity is approximate zero. In other words, no matter how much the S-wave velocity varies, no

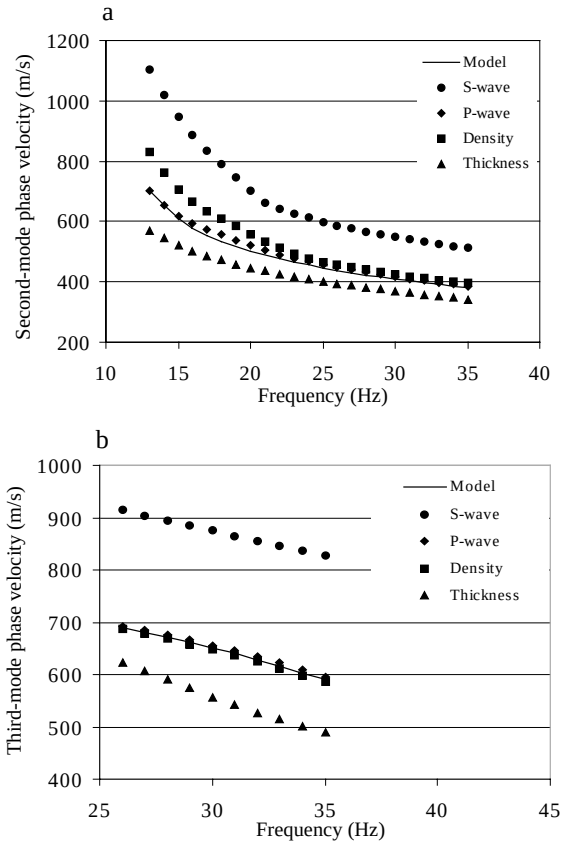

Fig. 3. Contribution to the second mode (a) and the third mode (b) Rayleigh-wave phase velocity by a 25% change in each earth parameter (Fig. 2). The solid line presents phase velocities caused by the earth model of Fig. 2. A 25% change in S-wave velocity causes a 40% change in the second mode phase velocities (solid dots) and a 36% change in the third mode phase velocities. A 25% change in density causes only slight change in the second mode phase velocities and visually no changes in the third mode phase velocities. A 25% change in P-wave velocity almost does not affect phase velocities.

changes in the phase velocity at that particular frequency can be observed. The open circles in Fig. 4 are the normalized row vectors of the Jacobian matrix associated with the shortest wavelength data of the layered earth model (Fig. 2). Each point in Fig. 4 represents sensitivity for a Rayleigh wave component

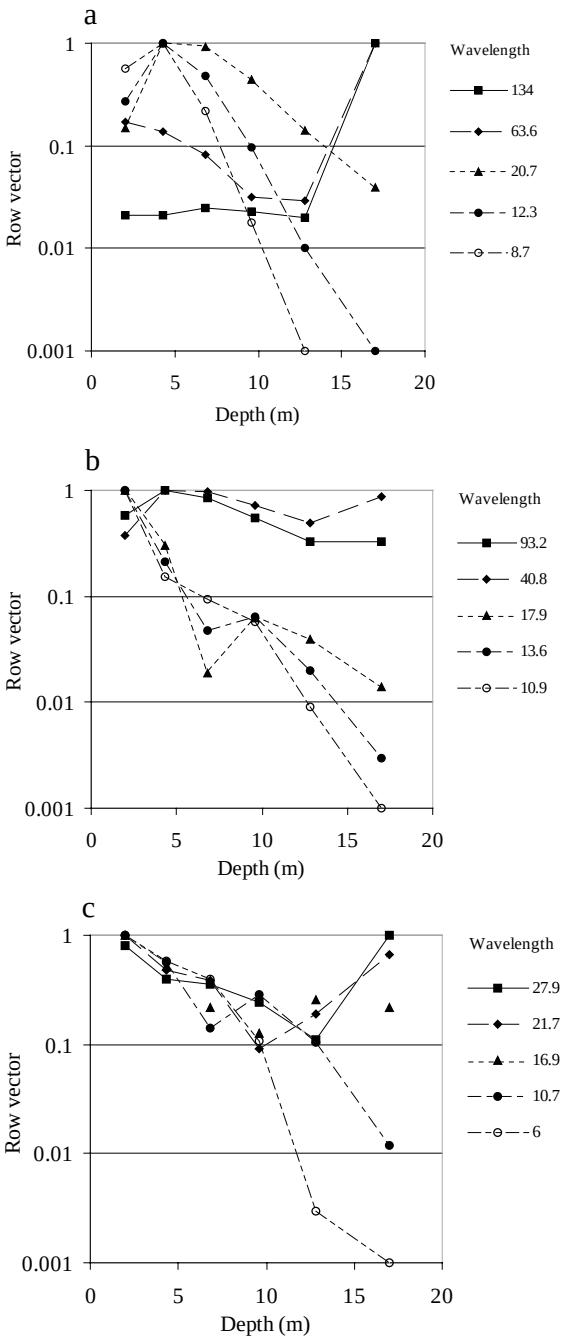

Fig. 4. Normalized row vectors of the Jacobian matrix show data sensitivity varying with depth: (a) the fundamental mode, (b) the second mode, and (c) the third mode. The vectors indicate the penetrating depth of each particular component of surface waves. For example, the maximum penetrating depth for a component of the fundamental mode surface wave with wavelength of 8.7 m (open circles in (a)) is approximately 13 m.

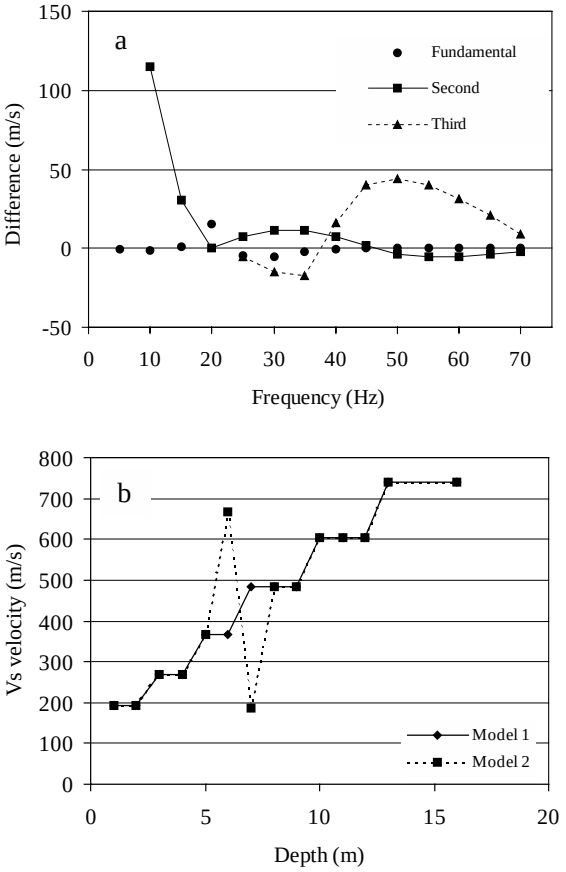

Fig. 5. Differences in phase velocities (a) due to models 1 and 2 (b). More than 100% difference in S-wave velocity models at depths of 6 and 7 m (b) results in a standard deviation of only 4.6 m/s in the fundamental mode data (a). The changes, however, cause standard deviations of 33.5 and 27.3 m/s for the second mode data and the third mode data, respectively.

with a certain wavelength at a particular depth. For example, in Fig. 4b, a 17.9-m component is more sensitive at a depth of 10 m than at a depth of 7.5 m. In Fig. 4a, a wavelength of 8.7 m is reaching zero at a depth of 13 m for the fundamental mode data. This means that the maximum penetrating depth for this component of surface waves is less than 13 m. In order to "see" a depth of 17 m, a wavelength of 12.3 m is required for fundamental mode data (a solid circle in Fig. 4a). However, for the second mode data, a component with a wavelength of 10.9 m can penetrate a depth of 17 m (Fig. 4b) or for the third mode data, a component with a wavelength of only 6 m can "see" a depth of 17 m (Fig. 4c). Based on analysis of row vectors of the Jacobian matrix, we concluded that high-mode Rayleigh-wave data can see" deeper (longer than the wavelength) when compared to the same wavelength components of the fundamental mode Rayleigh-wave data (normally shorter than the wavelength).

Most significant in this finding is that higher mode data stabilize the inversion process and increase the resolution of inverted S-wave velocities. Fig. 5 shows the difference in phase velocities (Fig. 5a) calculated from two S-wave velocity models (Fig. 5b). Although relative differences between S-wave velocities of model 1 and model 2 at depths of 6 and 7 m are more than 100%, the standard deviation between the

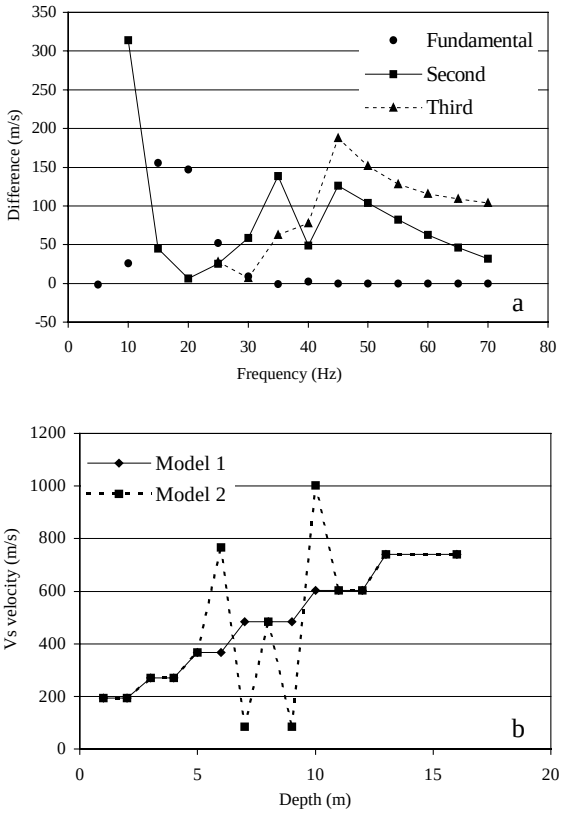

Fig. 6. Differences in phase velocities (a) due to models 1 and 2 (b). More than 100% difference in S-wave velocity models at depths of 6, 7, 9, and 10 m (b) results in a standard deviation of only 59 m/s in the fundamental mode data (a). The changes, however, cause standard deviations of 113 and 110 m/s for the second mode data and the third mode data, respectively.

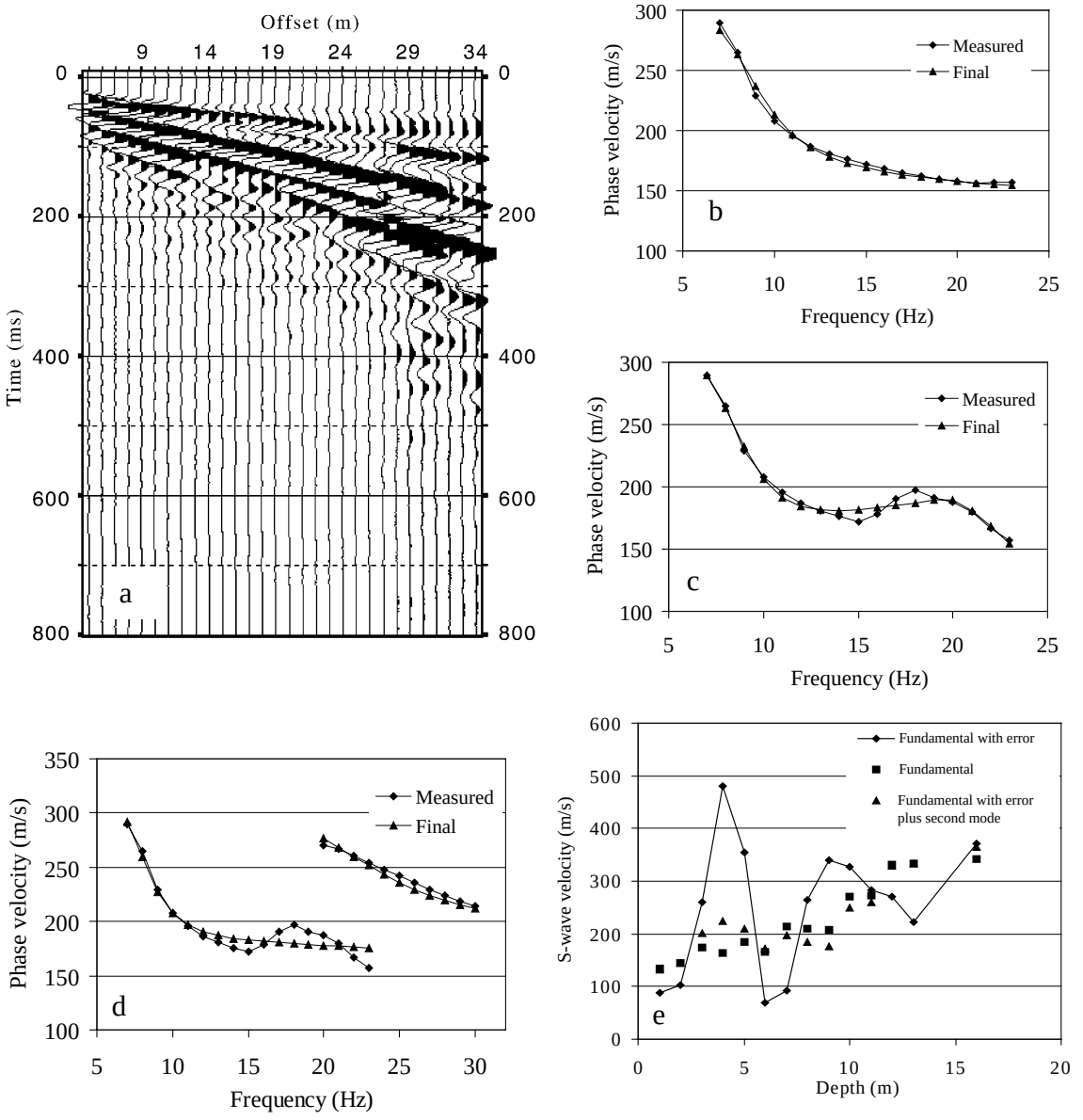

Fig. 7. An example from San Jose, CA. (a) Row surface-wave data and its image in the frequency-velocity domain shown in Fig. 1. (b) The accurate fundamental mode phase velocity. Phase velocities labeled "Measured" are extracted from Fig. 1 and labeled "Final" are calculated based on the S-wave velocity model marked by solid squares in (e). (c) The erroneous fundamental mode phase velocities. Phase velocities labeled "Measured" are extracted from Fig. 1 with noise deliberately introduced in the frequency range from 13 to 19 Hz. The data labeled "Final" are calculated based on the S-wave velocity model marked by diamonds with a solid line in (e). (d) The erroneous fundamental mode and the second mode phase velocities. Phase velocities labeled "Measured" are the same as (c) and higher mode data from 20 to 30 Hz are extracted from Fig. 1. The data labeled "Final" are calculated based on the S-wave velocity model marked by solid triangles in (e). (e) Inverted S-wave velocity profiles. Accurate fundamental mode data (b) yielded a smoothed S-wave velocity model (solid squares). The inversion of the erroneous fundamental mode data (c) produced an "irrational" model (diamonds with a solid line). A well-behaved S-wave velocity model (solid triangles) was found, because higher mode data from 20 to 30 Hz (d) were included in the inversion process. This S-wave velocity model was similar to the S-wave velocity model (solid squares) inverted from the accurate fundamental mode data.

fundamental mode phase velocities calculated from these two models is only 4.6 m/s. This indicates that the inversion process will choose either one of the models to be a final result at a 4.6 m/s error level. In practice, the "irrational" model 2 (solid squares with a dash line in Fig. 5b) could be selected if the inversion process is forced to conclude with an error level less than or equal to 4.6 m/s. However, because the standard deviations are 33.5 m/s for the second mode (solid squares with a solid line in Fig. 5a) and 27.3 m/s for the third mode data (solid triangles with a dash line in Fig. 5a), an inversion with high-mode data will reject "irrational" model 2 so that a stabilized inversion is achieved. Basically, the larger difference in higher modes suggests that higher modes are more sensitive to the changes in S-wave velocities than is the fundamental mode.

We can examine this property again with Fig. 6. A 100% difference in S-wave velocity models at depths of 6–10 m only results in a standard deviation of 59 m/s in the fundamental mode data (Fig. 6a). This indicates that the inversion process will choose either as a final result at a 59 m/s error level. The "irrational" model 2 (solid squares with a dash line in Fig. 6b) could be an inversion candidate, when the inversion process is forced to conclude with an error level less than 59 m/s. The "irrational" model 2, however, will be rejected if an inversion is performed with high-mode data because the standard deviations are 113 m/s for the second mode data and 110 m/s for the third mode data (Fig. 6a).

In conclusion, for higher mode Rayleigh-wave data, the S-wave velocity is still the dominant influence on dispersion curves. Furthermore, higher modes are relatively more sensitive to changes in S-wave velocity than is the fundamental mode. The Jacobian matrix of the higher mode Rayleigh-wave data suggests higher mode data have deeper investigation depths than do fundamental mode data. Because of limitations of resolution with the fundamental mode data, they are not sensitive to changes in S-wave velocities of conjunct layers, which deviate from the true values in opposite directions. An inversion performed with only fundamental mode data may accept the "irrational" model (Figs. 5b and 6b) due to its lower standard deviation. A simultaneous inversion of fundamental and higher mode data, however, definitely rejects the "irrational" model due to its higher standard deviation in higher modes. A stabilized inversion can be achieved by including higher mode data in an inversion process. The results depicted in Figs. 5a and 6a also show that large differences appear in relatively lower frequency ranges for the second modes and in relatively higher frequency ranges for the third modes. This feature could be utilized to increase resolution of an S-wave velocity model when defining the thickness of each layer based on availability of higher modes.

3. Real world examples of utilizing higher mode surface-wave data

3.1. San Jose, CA

A shallow high frequency surface wave survey was conducted in San Jose, CA, in 1998 to determine shear-wave velocities in near-surface materials up to 10 m deep. Thirty-channel vertical-component data were acquired by the MASW method. Thirty 4.5 Hz vertical-component geophones were used on a 1 m geophone interval and a 60-channel Geometrics StrataView seismograph. Vertical impacts from a 6.3 kg (14 lb) hammer on a metal plate provided the seismic energy. A record length of 1024 ms at a 1 ms sample interval was selected. The nearest geophone-source offset was 5 m. Raw field data are shown in Fig. 7a and its image in the

Fig. 8. An example from Vancouver, Canada. (a) Forty-eight channel raw surface-wave data. (b) The image of raw data (a) in the frequency-velocity domain. The fundamental and the second mode dispersion curves are clearly shown in this image. (c) The fundamental mode phase velocity. Phase velocities labeled "Measured" are extracted from (b) and labeled "Final" are calculated based on the S-wave velocity model marked by diamonds with a solid line in (e). (d) The fundamental mode phase velocity and higher mode data from 16 to 26 Hz. Phase velocities labeled "Measured" are extracted from (b) and labeled "Final" are calculated based on the S-wave velocity model marked by solid triangles in (e). (e) Inversion results. Inversion of the fundamental mode data alone can produce an "irrational" model (diamonds with a solid line). A well-behaved S-wave velocity model (solid triangles) was found, because higher mode data from 17 to 27 Hz (d) were included in the inversion process. This S-wave velocity model was confirmed by direct borehole measurements (solid squares).

frequency–velocity domain is shown in Fig. 1. High modes were evident in Fig. 1. We can confidently determine the second mode started at 20 Hz. The hole (weak energy) centered at 17 Hz and 300 m/s separates the second mode from another energy peak (12 to 15 Hz with velocities>300 m/s) that more than likely is calculation artifacts. We can also identify the third mode started at 35 Hz.

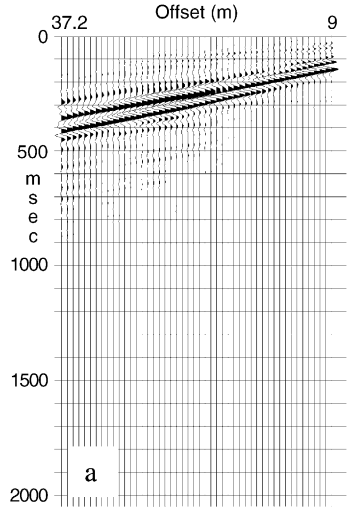

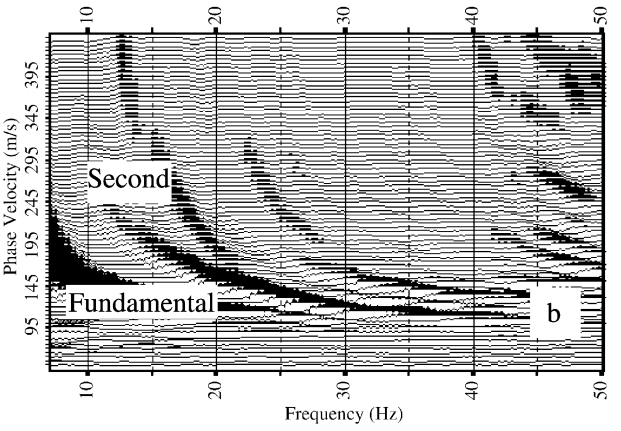

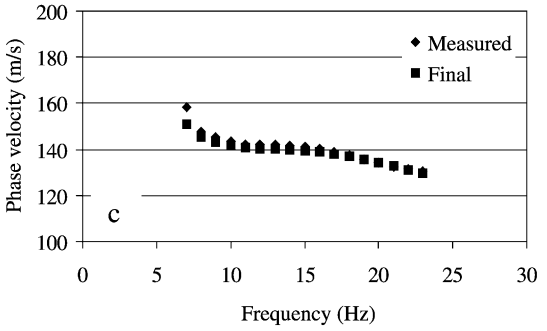

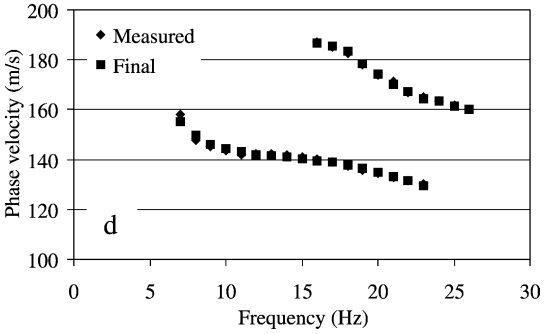

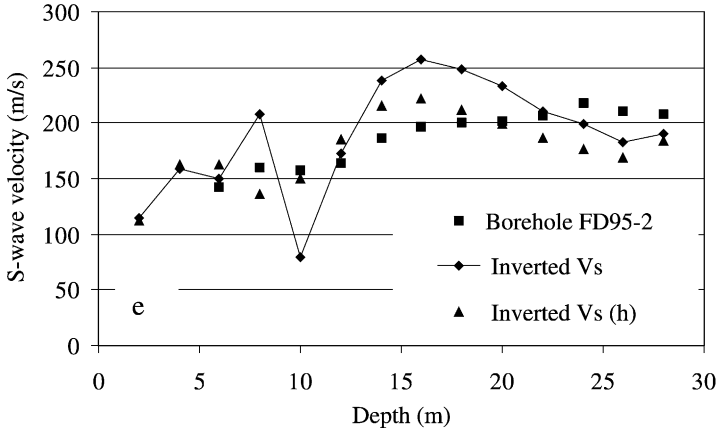

Three data sets were generated and inverted for comparison. The first set was fundamental mode surface wave data only (Fig. 7b), automatically extracted from Fig. 1 by SurfSeis© (a commercial software package developed at the Kansas Geological Survey). The second data set was fundamental mode data with noise deliberately introduced in the frequency range from 13 to 19 Hz (Fig. 7c). Noises were determined experimentally to simulate a case where the fundamental mode data are contaminated with higher modes and/or body waves. Based on our experience, the shape of the second data set as shown here is commonly seen in real data. The standard deviation between these two data sets is only 16 m/s. The third data set included the second set (noisy data) and the second mode surface wave data (Fig. 7d). A 14-layer model with each layer 1 m thick was chosen to test these three data sets.

Fig. 7e shows inverted S-wave velocities from all three data sets. All root-mean-square (rms) errors between the measured dispersion curve and calculated dispersion curves (Fig. 7b,c,d) from each of these S-wave velocity models (Fig. 7e) are less than 5 m/s. Because the fundamental mode data (Fig. 7b) were accurately extracted from Fig. 1, the inverted S-wave velocities (solid squares in Fig. 7e) were geologically reasonable. They smoothly increase from shallower layers to deeper layers. However, smoothness disappears when data set two (Fig. 7c) was inverted. The S-wave velocity model (diamonds with a solid line) changes irrationally in the depth range from 3 to 7 m. This instability is caused by forcing the response of the inverted model to fit the error. In the real world, it is common to provide an error range that will force an inverted model into an unreasonable space. We have experienced this situation a number of times when processing surface wave data. Better results are obtained when higher mode surface wave data (Fig. 7d) are inverted simultaneously with the fundamental mode data. Because of the higher rms error in the calculated second mode data, the S-wave velocity model with abrupt variation (diamonds with a solid line) was rejected. Inverted S-wave velocities (solid triangles) that included the second modes during inversion were similar to the results obtained from data set one (solid squares).

3.2. Vancouver, Canada

A test program, designed to evaluate the accuracy and efficiency of the MASW method (Park et al., 1999a; Xia et al., 1999) in an area with well founded and extremely high quality ground truth (Hunter et al., 1998), was established at the Fraser River delta, near Vancouver, British Columbia, Canada in 1998 (Xia et al., 2000 and 2002a). Surface wave data acquired at borehole FD95-2 (Fig. 8a) are used as an example to illustrate how inversion can be stabilized with higher mode data. Multi-channel surface wave data (Fig. 8a) were acquired using 4.5 Hz vertical geophones and a 48-channel Geometrics StrataView seismograph. Geophones were deployed at a 0.6 m interval with the source-to-nearest geophone offset of 9 m. A record length of 2048 ms at a 1 ms sample interval was selected, thus insuring the entire surface wavetrain was recorded. Three impacts were vertically stacked from an accelerated weight drop designed and built by the KGS. High modes were clearly shown in the frequency–velocity domain (Fig. 8b).

The fundamental mode phase velocities of surface waves from 7 to 23 Hz (diamonds in Fig. 8c) were automatically extracted from Fig. 8b by SurfSeis©. The sampling interval of surface wave data is 0.5 Hz in this example. For illustration purposes, surface wave data are plotted in a 1-Hz interval in Fig. 8c and d. At lower frequencies ($\sim$ 5 Hz, for this example), the resolution of dispersion curves in the frequency–velocity domain is relatively low so that phase velocity picking in a lower frequency range normally results in large errors. When surface wave energy is weak and/or possibly contaminated by other features, for example in the range $f < 17$ and $f > 27$ Hz for the second mode (Fig. 8b), it is difficult to pick phase velocities accurately. In practice, we used a trial-and-error method to find a proper frequency range.

As discussed in the previous section, inversion of fundamental mode data may result in an unrealistic S-wave velocity model due to limitations of resolution with the fundamental mode data. One potential S-wave velocity model (diamonds with a solid line in Fig. 8e) can be obtained by inverting only the fundamental mode data. Although the modeled surface-wave data (solid squares in Fig. 8c) from this S-wave velocity model fit the measured surface-wave data almost perfectly, this S-wave velocity model pos-

sessed a general pattern of oscillation and two extreme values. One extreme was at depth 8 m, a 30% higher than the borehole measurement, and the other at 10 m, a 50% lower than the borehole measurement (solid squares in Fig. 8e, Hunter et al., 1998). This S-wave velocity model was rejected when the second mode data (Fig. 8d) from 16 to 26 Hz were included in the inversion process and inverted simultaneously with the fundamental data. The inversion converged to a smoothed S-wave velocity model (solid triangles in Fig. 8e). This smoothed S-wave velocity model was confirmed by direct borehole measurements (Hunter et al., 1998).

4. Discussion

The errors in the inverted S-wave velocities (e.g., diamonds with a solid line in Figs. 7e and 8e) are caused by errors in dispersion data. For any noisy data, it is critical to define an appropriate error level and to terminate the inversion process at or a little above the error level to prevent transferring errors in data into inverted models. In most cases, the best fitting data does not necessarily yield the best inverted result.

We have shown that the inversion process is more stable when including higher mode data in the inversion of surface wave data. This stability indeed improves the resolution of inversion results. In the real world, what should we do if no higher modes are available? We have to make a choice between error and resolution of an inverted model. Sacrificing resolution, or a trade-off between resolution and error of a model, to obtain stable results is a wise strategy (Backus and Gilbert, 1970). We can reduce the error in the inverted S-wave velocity model by reducing the resolution of the model (increasing thickness of layers). In the San Jose example, we inverted data set two again with a 7-layer model, each layer being 2 m thick. This possesses only half the resolution of the previous model (1 m thick in Fig. 7e). Data set two (diamonds with a solid line in Fig. 9a) underwent the same inversion procedure used for the San Jose example (Fig. 7). Clearly, the inverted S-wave velocity model with the reduced resolution (diamonds with a solid line Fig. 9b) was more smoothed and acceptable geologically in comparison to the inverted mode depicted by diamonds with a solid line (Fig. 7e).

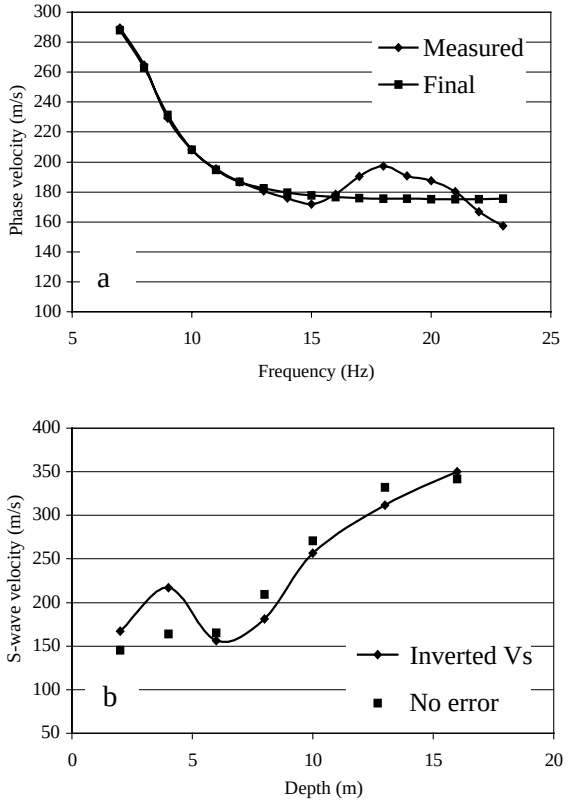

Fig. 9. The example shown in Fig. 7 with reduced resolution. Phase velocities (a) labeled "Measured" are extracted from Fig. 1. Phase velocities (a) labeled "Final" are calculated based on a stable and smoothed S-wave velocity model (diamonds with a solid line in (b)). The geologically acceptable and smoothed S-wave velocity model was obtained by reducing resolution from 1 (in Fig. 7e) to 2 m. Solid squares represent inversion results of accurate fundamental mode data in Fig. 7e.

5. Conclusions

Experimental analysis indicates that energy of higher modes tends to become more dominant as the source distance becomes larger. In some cases, higher mode data are necessary since shorter wavelength components of fundamental mode Rayleigh waves are obscured by these higher frequency data where higher modes of Rayleigh waves dominate. Our modeling results and real examples demonstrate that higher

mode data have a deeper investigation depth than fundamental mode data do. They also showed that higher mode data stabilize the inversion procedure and increase the resolution of inverted S-wave velocities. Because the resolution of an inverted model is generally determined by the accuracy of the data, we can determine the resolution of inverted S-wave velocities by forward modeling or by inverting synthetic surface wave data that contain deliberate errors. This research is the first attempt to utilize properties of higher modes to obtain near-surface S-wave velocities by inverting high-frequency surface wave data.

Acknowledgements

The authors thank the Geological Survey of Canada and Geometrics, for their support in acquiring surface wave data used as examples in this paper. We thank James Hunter and Ron Goods of the Geological Survey of Canada; James Harris of Millsaps College; Rob Huggins, Craig Lippus, Ming-Wen Sung, and Mark Prouty of Geometrics for their valuable discussions on surface wave techniques. We also thank two anonymous reviewers for their critical and constructive opinions that improved the manuscript. We appreciate the efforts of Mary Brohammer and Julia Shuklaper in preparation of this manuscript.

References

Aki, K., Richards, P.G., 1980. Quantitative seismology. Freeman, San Francisco.

Babuska, V., Cara, M., 1991. Seismic anisotropy in the earth. Kluwer Academic Publishing, Boston.

Backus, G.E., Gilbert, J.F., 1970. Uniqueness in the inversion of gross earth data. Philos. Trans. R. Soc. Lond., Ser., A 266, 123–192.

Craig, R.F., 1992. Soil mechanics, 5th ed. Chapman & Hall, New York.

Dorman, J., Ewing, M., 1962. Numerical inversion of seismic surface wave dispersion data and crust–mantle structure in the New York-Pennsylvania area. J. Geophys. Res. 67, 5227–5241.

Garland, G.D., 1979. Introduction to Geophysics: Mantle, Core and Crust, 2nd ed. W.B. Saunders, Philadelphia.

Glangeaud, F., Mari, J.L., Lacoume, J.L., Mars, J., Nardin, M., 1999. Dispersive seismic waves in geophysics. Eur. J. Environ. Eng. Geophys. 3, 265–306.

Grant, F.S., West, G.F., 1962. Interpretation theory in applied geophysics. McGraw-Hill, New York.

Hunter, J.A.M., Burns, R.A., Good, R.L., Pelletier, C.F., 1998. A compilation of shear wave velocities and borehole geophysical logs in unconsolidated sediments of the Fraser River delta. Geological Survey of Canada, Open File No. 3622, available on CD-ROM.

Imai, T., Tonouchi, K., 1982. Correlation of N-value with S-wave velocity and shear modulus. Proceedings, 2nd European Symposium on Penetration Testing, Amsterdam. A.A. Balkema Publishers, Netherlands, pp. 57–72.

Kovach, R.L., 1965. Seismic surface waves: some observations and recent developments. In: Ahrens, L.H., Frank Press, Runcorn, S.K., Urey, H.C. (Eds.), Physics and Chemistry of the Earth, vol. 6. Pergamon Press, Oxford, pp. 251–314.

Malagnini, L., Hermann, R.B., Biella, G., de Franco, R., 1995. Rayleigh wave in Quaternary alluvium from explosive sources: determination of shear-waves velocity and Q structure. Bull. Ses. Soc. Am. 85, 900–922.

Matthews, M.C., Hope, V.S., Clayton, C.R.I., 1996. The use of surface waves in the determination of ground stiffness profiles. Proc. I.C.E., Geotech. Eng. 119 (2), 84–95, Thomas Telford Ltd., London.

Miller, R.D., Xia, J., Park, C.B., Ivanov, J., 1999. Multichannel analysis of surface waves to map bedrock. Lead. Edge 18, 1392–1396.

Park, C.B., Miller, R.D., Xia, J., 1996. Multi-channel analysis of surface waves using vibroseis (MASWV). Exp. Abstrs. of Technical Program with Biographies, Society of Exploration Geophysicists, 66th Annual Meeting, Denver, Colorado. Society of Exploration Geophysicists, Tulsa, OK, pp. 68–71.

Park, C.B., Miller, R.D., Xia, J., 1998. Imaging dispersion curves of surface waves on multi-channel record. Exp. Abstrs. of Technical Program with Biographies, Society of Exploration Geophysicists, 68th Annual Meeting, New Orleans, Louisiana. Society of Exploration Geophysicists, Tulsa, OK, pp. 1377–1380.

Park, C.B., Miller, R.D., Xia, J., 1999a. Multi-channel analysis of surface waves (MASW). Geophysics 64, 800–808.

Park, C.B., Miller, R.D., Xia, J., 1999b. Multimodal analysis of high frequency surface wave. Proceedings of the Symposium on the Application of Geophysics to Engineering and Environmental Problems (SAGEEP 99), Oakland, CA, March 14-18. Environmental and Engineering Geophysical Society, Wheat Ridge, Colorado, USA, pp. 115–122.

Park, C.B., Miller, R.D., Xia, J., Hunter, J.A., Harris, J.B., 1999c. Higher mode observation by the MASW method. Exp. Abstrs. of Technical Program with Biographies, Society of Exploration Geophysicists, 69th Annual Meeting, Houston, TX. Society of Exploration Geophysicists, Tulsa, OK, pp. 524–527.

Press, W.H., Teukosky, S.A., Vetterling, W.T., Flannery, B.P., 1992. Numerical recipes in C, 2nd ed. Press Syndicate of the University of Cambridge, New York.

Rayleigh, L., 1885. On waves propagated along the plane surface of an elastic solid. Proc. Lond. Math. Soc. 17, 4.

Schwab, F.A., Knopoff, L., 1972. Fast surface wave and free mode computations. In: Bolt, B.A. (Ed.), Methods in Computational Physics. Academic Press, New York, pp. 87–180.

Sheriff, R.E., 1991. Encyclopedic dictionary of exploration geophysics, 3rd ed. Society of Exploration Geophysicists, Tulsa, OK.

Stokoe II, K.H., Nazarian, S., 1983. Effectiveness of ground improvement from Spectral Analysis of Surface Waves. Proceeding of the Eight European Conference on Soil Mechanics and Foundation Engineering, Helsinki, Finland.

Stokoe II, K.H., Wright, S.G., Bay, J.A., Roësset, J.M., 1994. Characterization of geotechnical sites by SASW method. In: Woods, R.D. (Ed.), Geophysical Characterization of Sites, ISSMFE Technical Committee #10. Oxford Publishers, New Delhi, pp. 15–25.

Xia, J., Miller, R.D., Park, C.B., 1997. Estimation of shear wave velocity in a compressible Gibson half-space by inverting Rayleigh wave phase velocity. Exp. Abstrs. of Technical Program with Biographies, Society of Exploration Geophysicists, 67th Annual Meeting, Dallas, TX. Society of Exploration Geophysicists, Tulsa, OK, pp. 1917–1920.

Xia, J., Miller, R.D., Park, C.B., 1998. Construction of vertical section of near-surface shear-wave velocity from ground roll. Exp. Abstrs. of Technical Program, The Society of Exploration Geophysicists and The Chinese Petroleum Society Beijing 98' International Conference. Chinese Petroleum Society, Beijing, pp. 29–33.

Xia, J., Miller, R.D., Park, C.B., 1999. Estimation of near-surface shear-wave velocity by inversion of Rayleigh wave. Geophysics 64, 691–700.

Xia, J., Miller, R.D., Park, C.B., Hunter, J.A., Harris, J.B., 2000. Comparing shear-wave velocity profiles from MASW with borehole measurements in unconsolidated sediments, Fraser River Delta, B.C., Canada. J. Environ. Eng. Geophys. 5 (3), 1–13.

Xia, J., Miller, R.D., Park, C.B., Hunter, J.A., Harris, J.B., Ivannov, J., 2002a. Comparing shear-wave velocity profiles from multichannel analysis of surface wave with borehole measurements. Soil Dyn. Earthqu. Eng. 22 (3), 181–190.

Xia, J., Miller, R.D., Park, C.B., Wightman, E., Nigbor, R., 2002b. A pitfall in shallow shear-wave refraction surveying. J. Appl. Geophys. 51 (1), 1–9.